Available online at www.sciencedirect.com
SCIENCE DIRECT®
Physics Letters A 331 (2004) 332–336
PHYSICS LETTERS A
www.elsevier.com/locate/pla

Structures and properties of Ni nanowires

H.Y. Zhang, X. Gu, X.H. Zhang, X. Ye, X.G. Gong *

Surface Physics Laboratory and Department of Physics, Fudan University, Shanghai 200433, China

Received 4 April 2004; received in revised form 12 August 2004; accepted 13 August 2004

Available online 26 August 2004

Communicated by R. Wu

Abstract

Atomic structures and vibrational density of states of Ni nanowire are studied by using the generalized simulated annealing method. Compact, helical and amorphous-like structures are found for different wire lengths. Molecular dynamics simulations at finite temperature confirm the thermal stability of these structures.

PACS: 61.46.+w

Keywords: Metal nanowire

1. Introduction

Increasing interest in nanoscience and nanotechnology has inspired a great deal of research on metal nanowires and nanotubes in recent years. Metal wires of several nanometers long with peculiar structures can be fabricated using various techniques [1–4]. It is well known that structures and properties of small entities are very different from those of bulk materials. For example, novel helical multi-shell structures have been identified both theoretically and experimentally [5–11]. Single-wall gold nanotubes were also observed very recently [6].

Various theoretical approaches have been applied to predict atomic structures of metal nanowires [12–20]. Noncrystalline structures with locally icosahedral packing have been found for thin Al and Pb nanowires through the molecular dynamics-based annealing simulations with empirical many-body interatomic potentials [21]. Interestingly, it was found that structures strongly depend on the diameter; structural transition from noncrystalline to the fcc structure takes place near a diameter of 3.0 nm for the Al and Pb wires. Nevertheless, most of the theoretical studies so far were performed for infinite long nanowires with a periodicity along the wire axis. The size dependence of structural properties has been rarely explored. It is hence important to explore the effects of wire length and mechanical loads.

* Corresponding author.
E-mail address: xggong@fudan.edu.cn (X.G. Gong).

0375-9601/$ – see front matter
doi:10.1016/j.physleta.2004.08.016

2. Theoretical methods

The simulated annealing method, one of the most powerful approachs for structural optimization tasks, is used to investigate the atomic structure of Ni wire in the present work. Traditionally, there are so-called classical simulated annealing (CSA) [22] and fast simulated annealing (FSA) [23]. The main difference between them is in the visiting distribution function. CSA and FSA can be further generalized according to the Tsallis statistics [24,25] within a unified picture to the so-called generalized simulated annealing algorithm (GSA) [26,27]. GSA uses a somewhat distorted Cauchy–Lorentz visiting distribution where the shape is controlled by a parameter q_v

$$g_{q_v}\big(\Delta x(t)\big) \propto \frac{[T_{q_v}(t)]^{-\frac{D}{3-q_v}}}{[1+(q_v-1)\frac{(\Delta x(t))^2}{[T_{q_v}(t)]^{2/(3-q_v)}}]^{\frac{1}{q_v-1}+\frac{D-1}{2}}}, \tag{1}$$

q_v also controls the rate of cooling as

$$T_{q_v}(t) = T_{q_v}(1)\frac{2^{q_v-1}-1}{(1+t)^{q_v-1}-1}, \tag{2}$$

where T_{q_v} is the visiting temperature.

A generalized Metropolis algorithm for the acceptance probability is used,

$$p_{q_a} = \min\big\{1, \big[1-(1-q_a)\beta\Delta E\big]^{\frac{1}{1-q_a}}\big\}, \tag{3}$$

where $\beta = \frac{1}{kT_{q_v}}$, and q_a controls the acceptance probability. For $q_a < 1$, zero acceptance probability is assigned to the case if

$$\big[1-(1-q_a)\beta\Delta E\big] < 0. \tag{4}$$

When $q_v = 1$ and $q_a = 1$, GSA recovers CSA; whereas if $q_v = 2$ and $q_a = 1$, GSA recovers FSA. When $q_v > 2$, the GSA cooling is faster than that of CSA and FSA. Since GSA has high possibilities for long jumps, it is more likely to find the global minimum with GSA than FSA or CSA.

In the present study, we choose an initial temperature corresponding to an acceptance probability of $\sim 86\%$; q_v and q_a are set to 2.62 and -5, respectively. In order to accelerate convergence, the acceptance temperature T_{q_a} is set to be equal to the visiting temperature T_{q_v} divided by time steps, i.e., $T_{q_a} = T_{q_v}/t$. Our tests show that this simple technique works equally well as our previous work which assumes linear decrease of q_a with the time steps [28–30]. For each initial configuration, we first perform GSA until the visiting temperature reaches 0.01, then use the conjugate gradient minimization scheme for refinements.

The Finnis–Sinclair (FS) potential, which is regarded as one of the best model potentials for transition metals [31], is used to model the atomic interaction in Ni wire. The Sutton–Chen version of this potential [32] has the form

$$V = \epsilon\sum_i\left[\frac{1}{2}\sum_{j\neq i}\left(\frac{a}{r_{ij}}\right)^n - c\rho_i^{1/2}\right], \tag{5}$$

where

$$\rho_i = \sum_{j\neq i}\left(\frac{a}{r_{ij}}\right)^m, \tag{6}$$

r_{ij} is the distance between the ith and jth atoms, a is the lattice constant, c is a dimensionless parameter, ϵ is the parameter with dimension of energy, and m, n are integers. The square root term in the attractive part of the potential accounts for many-body interactions. The parameters in the above equation for Ni are: $a = 3.52$ Å, $c = 39.432$, $\epsilon = 1.5707\times 10^{-2}$ eV, $m = 6$, and $n = 9$. Such a potential has been successfully used for Ni clusters [33]. As shown by Nayak et al. [34,35], the structures of small Ni clusters predicted by this potential are in good agreement with ab initio results.

3. Results and discussions

Our simulations start initially from the bulk-like structure, taking a number of atoms within a cylinder along [100], [110] and [111] directions of the fcc lattice. At first, the interlayer distance is taken as that in the bulk. The infinite length of wire is modelled by a supercell with periodic boundary condition along the wire axis. Fig. 1 shows that the structure obtained by the generalized simulated annealing method. From the figure, one can have two basic observations. First, the structure is size (radius)-dependent. The structures studied here have 5 to 19 atoms in each layer. The very thin nanowire prefers helical structure, while the relatively large one adopts compact structure, with a

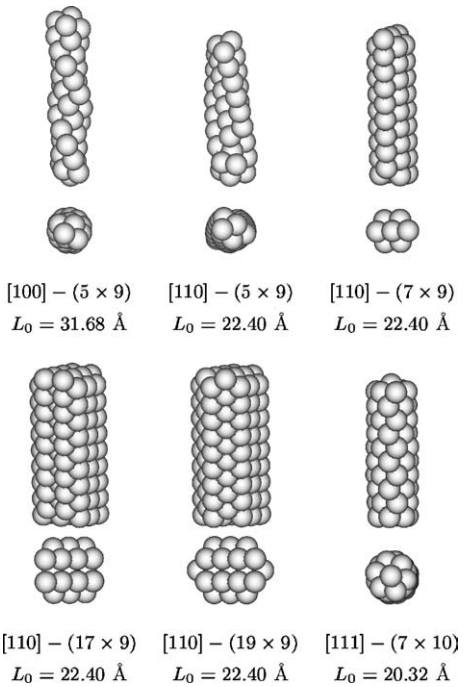

Fig. 1. Schematic structure of Ni nanowires with different initial configurations. Label $[n_1n_2n_3]$–$(m_1 \times m_2)$ indicates that m_2 layers along $[n_1n_2n_3]$ direction with m_1 atoms in each layer.

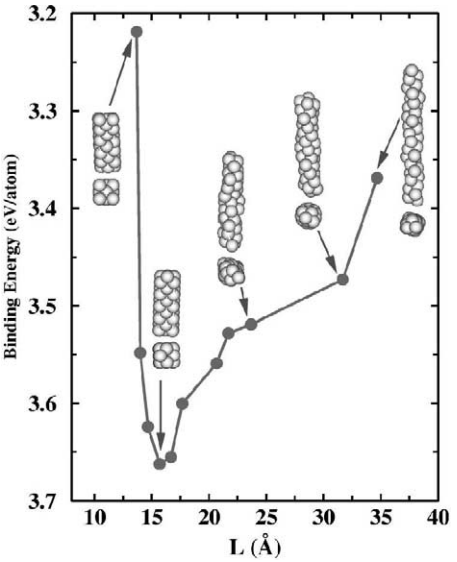

Fig. 2. The relative binding energy as a function of the wire length for the relaxed structure of [100]–(5 × 9) nanowire. The initial length is 31.68 Å. Some selected morphologies are also shown.

polygon cross section. In the [110]–(19 × 9) wire (see the caption of Fig. 1 for the definition of the label), for example, the cross section is hexagonal-like. We did not find multi-shell structures in the present study, different from previous observations for nanowires a few nanometers wide [2,21]. The reason can be that present model is too small to produce multishell structures. Second, it is easy to find structural differences between the [100]–(5 × 9) and [110]–(5 × 9) wires, although both are helical-like. If the initial orientation of wire does not play any important role for the final structure of nanowire, the only difference of the initial configurations between these two nanowires must be in the length of the supercell. Therefore, these structural differences suggest that the length of the supercell will also strongly affect the structure of the nanowire.

The structural changes with the length of the supercell have been studied. While the length of the supercell increases, the wire becomes thinner, and more defects appear on the surface. One can expect that, the chain will finally break. By contrast, the structure becomes more compact, and helical feature of the structure also disappears gradually (see Fig. 2), and at the same time the binding energy increases quickly when the length decreases. When shortened by approximately 50% to about 15.7 Å, the wire becomes energetically the most stable. If the length of the supercell decreases further, the binding energy decreases sharply, like in a strong repulsive region. Although the morphology of the wire does not change significantly, the bond length and bond angle have changed as discussed below.

To give more information on the structural properties, we show the pair correlation function (PCF) for the [100]–(5 × 9) and [111]–(7 × 10) nanowires in Fig. 3. It can be seen that, PCF shows a strong length-dependence. It is interesting to note that, at the initial length 31.68 Å of the [100]–(5 × 9) wire, there is only one peaks at 2.4 Å, corresponding to the first nearest neighbor distances in the bulk Ni. However, one can find a new peak near 4.0 Å, which indicates special structures in wire. When the length decreases to 23.68 Å, no obvious structural change occurs despite small alternations in the second neighbors. When the wire is compressed further, the PCF changes significantly. The first peak splits into two; meanwhile two sharp peaks appear at 3.2 and 3.6 Å, indicating cor-

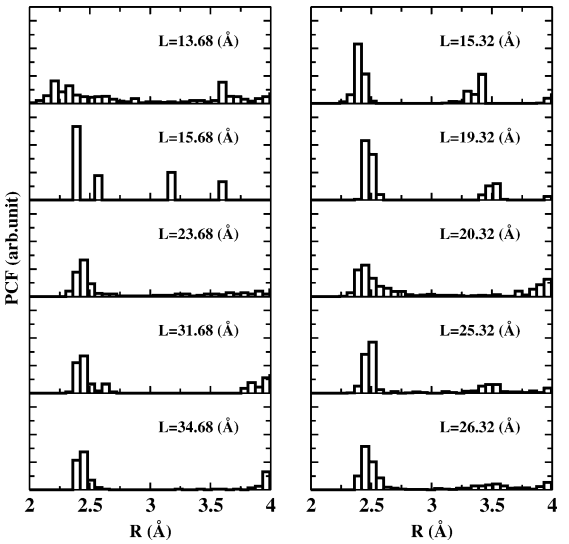

Fig. 3. Pair correlation function of Ni nanowire at different wire length. Left panel for [100]–(5 × 9) and right panel for [111]–(7 × 10) nanowire.

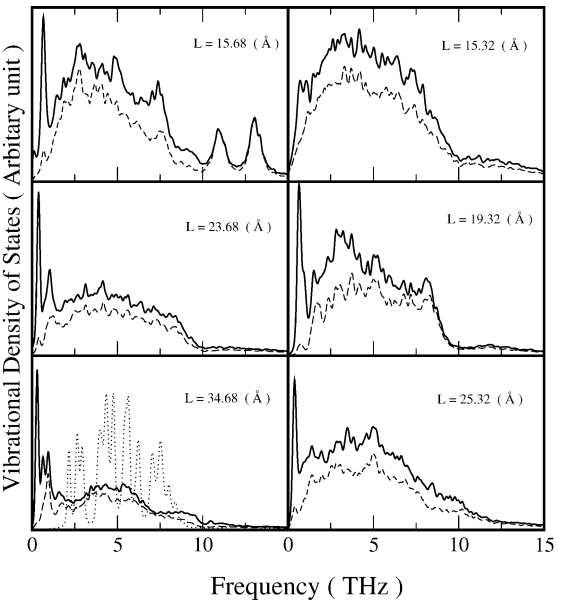

Fig. 4. Vibrational density of state of selected structures for the Ni nanowire (solid line). The dashed line is for the modes vibrating along the axis of the wire, and the dotted line in the button-left panel is for the bulk Ni.

relation between an ordered structure and the highest binding energy. Amorphous-like structures gradually develops when the wire is compressed more, as suggested by broad PCF features in the top-left panel of Fig. 3. Typically, structural disordering reduces binding energy, in accordance with Fig. 2.

The PCF also clearly shows structural difference for nanowires with various initial configurations. The PCF of the [111]–(7 × 10) nanowire is very different from that of the [100]–(5 × 9) wire. In Fig. 3, one can clearly see the first peak near 2.5 Å and the second peak near 3.5 Å for [111]–(7 × 10) wire, corresponding to the first and the second nearest neighbor distances, respectively. Such PCF also indicates that the structure of wire has the compact feature, different from the helical structure.

To understand the physical properties of the wires at finite temperature, we have performed the microessemble molecular dynamics simulation. The temperature is set to approximately 200 K. The integration is made by the Verlet algorithm, with a time duration of 100 ps and a time step of 1 fs. The simulations indicate that the structures obtained by the GSA approach is stable, no significant structural change was found during MD simulations.

Through Fourier transformation of velocity–velocity auto correlation function, we got the vibrational density states (VDOS) for all the optimized structures, as shown in Fig. 4. Comparing with the VDOS of the bulk Ni, the most significant changes appear in both low and high frequency region. Generally speaking, the VDOS in the low frequency part increases with length expansion, due to the reduction in force constants. In contrast, the high frequency part of the VDOS enhances in compressed structures with larger force constants. In the low frequency region, the VDOS of three-dimensional solid is proportional to the square of frequency, while in nanoclusters, it should display a linear behavior [36]. For the present nanowires, except for an overall increasing of the density of states in the low frequency region, we have found a unusually high peak at ~ 0.07 THz. This has never been reported before for other nanosystems, such as clusters. By carefully analyzing the vibrational modes, we find that this peak comes from collective motion perpendicular to the wire axis, like the vibration of a rope. In general, long and soft wires should display high VDOS peak of this collective mode. We believe this is an unique feature of the free standing nanowire.

4. Summary

We have studied the structures of thin Ni nanowires, with 5 to 19 atoms in the cross layer. The equilibrium structures show strong dependence on geometric conditions. All wires show energy minima at length much shorter than that initially taken from the crystalline solid. At the energy minima, atomic structures are quite compact and ordered. However, if the wires are compressed further, they become amorphous-like. The helical structure can appear only when the wire is much stretched. Comparing to the bulk Ni, VDOS is significantly different at low and high frequency region. A high peak has been identified at 0.07 THz for the collective motion, unique for free standing wires.

Acknowledgements

This work is supported by the National Science Foundation of China, the special funds for major state basic research.

References

[1] G. Bilalbegović, Phys. Rev. B 58 (1998) 15412.
[2] B.L. Wang, S.Y. Yin, G.H. Wang, A. Buldum, J.J. Zhao, Phys. Rev. Lett. 86 (2001) 2046.
[3] J.W. Kang, H.J. Hwang, Comput. Mater. Sci. 27 (2003) 305.
[4] A.I. Yanson, I.K. Yanson, J.M. van Ruitenbeek, Phys. Rev. Lett. 84 (2000) 5832.
[5] J.C. Wang, C.Z. Zhan, F.G. Li, Solid State Commun. 125 (2003) 629.
[6] Y. Oshima, A. Onga, Phys. Rev. Lett. 91 (2003) 205503.
[7] R. Hertel, J. Magn. Magn. Mater. 249 (2002) 251.
[8] K. Nielsch, R. Hertel, R.B. Wehrspohn, J. Barthel, J. Kirschner, U. Gösele, S.F. Fischer, H. Kronmüller, IEEE Trans. Magn. 38 (2002) 2571.
[9] M.S. Dresselhaus, Y.M. Lin, O. Rabin, A. Jorio, A.G. Souza Filho, M.A. Pimenta, R. Saito, Ge.G. Samsonidze, G. Dresselhaus, Mater. Sci. Eng. C 23 (2003) 129.
[10] O. Gülseren, F. Ercolessi, E. Tosatti, Phys. Rev. B 51 (1995) 7377.
[11] A. Pérez-Junquera, J.I. Martín, M. Vélez, J.M. Alameda, J.L. Vicent, Nanotechnology 14 (2003) 294.
[12] G.E. Tommei, F. Baletto, R. Ferrando, R. Spadacini, A. Danani, Phys. Rev. B 69 (2004) 115426.
[13] R.P. Wang, G. Xu, P. Jin, Phys. Rev. B 69 (2004) 113303.
[14] J. Diao, K. Gall, M.L. Dunn, Nat. Mater. 2 (2003) 656.
[15] X.L. Chen, Y.C. Lan, J.Y. Li, Y.G. Cao, M. He, J. Crystal Growth 222 (2001) 586.
[16] A.B. McLean, I.G. Hill, Appl. Surf. Sci. 162–163 (2000) 620.
[17] M.I. Chipara, R. Skomski, D.J. Sellmyer, J. Magn. Magn. Mater. 249 (2002) 246.
[18] V.V. Pogosov, D.P. Kotlyarov, A. Kiejna, K.F. Wojciechowski, Surf. Sci. 472 (2001) 172.
[19] F. Di Tolla, A. Dal Corso, J.A. Torres, E. Tosatti, Surf. Sci. 454–456 (2000) 947.
[20] H. Ikeda, Y. Qi, T. Cagin, K. Samwer, W.L. Johnson, W.A. Goddard III, Phys. Rev. Lett. 82 (1999) 2900.
[21] O. Gülseren, F. Ercolessi, E. Tosatti, Phys. Rev. Lett. 80 (1998) 3775.
[22] S. Kirkpatrick, C.D. Gelatt Jr., M.P. Vecchi, Science 220 (1983) 671.
[23] H. Szu, R. Hartley, Phys. Lett. A 122 (1987) 157.
[24] I. Andricioaei, J.E. Straub, Phys. Rev. E 53 (1996) 3055.
[25] C. Tsallis, J. Stat. Phys. 52 (1988) 479.
[26] C. Tsallis, D.A. Stariolo, Physica A 233 (1996) 395.
[27] T. Munakata, Y. Nakamura, Phys. Rev. E 64 (2001) 046127.
[28] Y. Xiang, D.Y. Sun, W. Fan, X.G. Gong, Phys. Lett. A 233 (1997) 216.
[29] Y. Xiang, D.Y. Sun, X.G. Gong, J. Phys. Chem. A 104 (2000) 2746.
[30] Y. Xiang, X.G. Gong, Phys. Rev. E 62 (2000) 4473.
[31] M.W. Finnis, J.E. Sinclair, Philos. Mag. B 50 (1984) 45.
[32] A.P. Sutton, J. Chen, Philos. Mag. Lett. 61 (1990) 139.
[33] J.P.K. Doye, D.J. Wales, New J. Chem. 22 (1998) 733.
[34] S.K. Nayak, S.N. Khanna, B.K. Rao, P. Jena, J. Phys. Chem. A 101 (1997) 1072.
[35] B.V. Reddy, S.K. Nayak, S.N. Khanna, B.K. Rao, P. Jena, J. Phys. Chem. A 102 (1998) 1748.
[36] D.Y. Sun, X.G. Gong, X.Q. Wang, Phys. Rev. B 63 (2001) 193412.